

Diphoton production in the ADD model to NLO+parton shower accuracy at the LHC

R. Frederix^a, Manoj K. Mandal^b, Prakash Mathews^c, V. Ravindran^b,
Satyajit Seth^c, P. Torrielli^a, M. Zaro^d

^a Institut für Theoretische Physik, Universität Zürich, Winterthurerstrasse 190,
CH-8057 Zürich, Switzerland

^b Regional Centre for Accelerator-based Particle Physics
Harish-Chandra Research Institute, Chhatnag Road, Jhansi,
Allahabad 211 019, India

^c Saha Institute of Nuclear Physics, 1/AF Bidhan Nagar, Kolkata 700 064, India

^d Centre for Cosmology, Particle Physics and Phenomenology (CP3)
Université Catholique de Louvain
Chemin du Cyclotron 2, B1348 Louvain-la-Neuve, Belgium

Abstract

In this paper, we present the next-to-leading order predictions for diphoton production in the ADD model, matched to the HERWIG parton shower using the MC@NLO formalism. A selection of the results is presented for $d = 2 - 6$ extra dimensions, using generic cuts as well as analysis cuts mimicking the search strategies as pursued by the ATLAS and CMS experiments.

1 Introduction

Extra dimension models [1, 2] are important new physics scenarios at the TeV scale that address the hierarchy problem and are being extensively studied at the LHC. Recently both ATLAS [3] and CMS [4] have looked for evidence of extra spatial dimension in the diphoton final state and put bounds on the fundamental Planck scale M_S in $(4 + d)$ -dimensions, for the 7 TeV proton-proton collision.

In the extra dimension models, Kaluza-Klein (KK) modes of a graviton (as a result of the graviton propagating in the extra dimensions), could decay to a pair of photons. Interaction of the massive spin-2, KK modes $h_{\mu\nu}^{(\vec{n})}$ with the standard model (SM) particles localised on a 3-brane, is *via* the energy momentum tensor $T^{\mu\nu}$ of the SM

$$\mathcal{L} = -\frac{\kappa}{2} \sum_{(\vec{n})} T^{\mu\nu}(x) h_{\mu\nu}^{(\vec{n})}(x), \quad (1)$$

where $\kappa = \sqrt{16\pi}/M_P$ is the reduced Planck mass in 4-dimensions. In process involving virtual exchange of KK modes between the SM particles, like in the diphoton production process, the sum of the KK mode propagator $\mathcal{D}(s)$ is given by

$$\begin{aligned} \kappa^2 \mathcal{D}(s) &= \kappa^2 \sum_n \frac{1}{s - m_n^2 + i\epsilon}, \\ &= \frac{8\pi}{M_S^4} \left(\frac{\sqrt{s}}{M_S} \right)^{(d-2)} \left[-i\pi + 2I \left(\frac{\Lambda}{\sqrt{s}} \right) \right], \end{aligned} \quad (2)$$

where s is the partonic center of mass energy, d is the compactified extra spatial dimensions, Λ is the UV cutoff of the KK mode sum which is usually identified as M_S [5, 6] and the integral $I(\Lambda/Q)$ is given in [5]. Note that in Eq. 2, we have included the κ^2 (suppression as a result of gravity coupling), which on summation over the high multiplicity of KK modes compensates the suppression in the ADD model. In this analysis we have followed the convention of [5].

Improved theoretical predictions to higher orders in QCD have now been performed for cross sections of pair production processes *viz.* di-lepton [7], di-gauge boson ($\gamma\gamma$ [8], ZZ and W^+W^- [9]), which in extra dimension models could result from the exchange of a virtual KK mode in addition to the usual SM contribution. The real emission of KK modes lead to large missing E_T signals *viz.* mono-jet [10], mono-photon [11], mono-Z boson, and mono- W^\pm boson [12]. The next to leading order (NLO) QCD corrections in some of the above processes are quite substantial and their inclusion in the computation also lead to a reduction of theoretical uncertainties, making it possible for the experiments to put more stringent bounds on the extra dimension model parameters.

The diphoton final state is an important signal for extra dimension searches, as the branching ratio of a KK mode decay to diphoton is twice than that of a decay

to individual charged lepton pair. The quantitative impacts of the NLO QCD correction to the diphoton final state for extra dimension searches have been studied in [8], where various infrared safe observable were studied using phase space slicing method. The factorisation scale dependence gets reduced when $\mathcal{O}(\alpha_s)$ corrections are included. Fixed order calculation truncated to NLO, at best yields results for sufficiently inclusive observable. Combining fixed order NLO and parton shower Monte Carlo (PS) [13, 14], would extend the coverage of the kinematical region to consistently include resummation in the collinear limit and also make a more exclusive description of the final state and get as realistic as possible to the experimental situation. The flexibility to incorporate hadronisation models and capabilities to simulate realistic final state configurations that can undergo detector simulations are the main advantage for the experimental collaborations.

ATLAS [3] and CMS [4] have analysed the diphoton invariant mass spectrum, using a constant K-factor for the full range of the invariant mass distribution to put lower bounds on extra dimension scale to NLO accuracy. However, this choice is not sensitive to possible distortions of distributions that can arise at NLO. Our present analysis will further help to put more stringent bounds on the model parameters. In this analysis we have considered various distributions for the ADD model parameters $d = 2$ to 6 with appropriate M_S value as bounded by the experiments [3, 4]. In Table 1, the M_S values for different extra dimensions d used in this analysis have been tabulated. For relevant observables we consider the fixed order results to NLO

d	2	3	4	5	6
M_S (TeV)	3.7	3.8	3.2	2.9	2.7

Table 1: M_S values used for the various extra dimensions d in our analysis.

accuracy and include PS. Factorisation, renormalisation scale uncertainties and PDF uncertainties are also estimated in an automated way [15]. For photon isolation, both smooth cone isolation and the experimental isolation criteria are considered.

The rest of the paper is organised as follows. In section 2, we discuss the NLO results to the diphoton final state in the ADD model and the essential steps needed to implement the parton showering to NLO accuracy. In section 3, we present selected numerical results and estimate the various theoretical uncertainties. Finally, in section 4 our conclusions are presented.

2 NLO + parton shower

Since the KK modes couple universally to the SM particles through the energy momentum tensor, both the $q\bar{q}$ and gg channel would contribute to the diphoton final state at leading order (LO). In the SM, the gg channel starts only at next to next to leading order (NNLO) *via* the finite box contribution through quark loop and the

large gluon-gluon flux at the LHC makes this contribution potentially comparable to the LO results. In the invariant mass region of interest to extra dimension searches, the box diagram contribution is not significant enough [8].

All the partonic contributions to NLO in QCD have been calculated for the diphoton final state [8], for both large (ADD) [1] and warped (RS1) [2] extra dimension models. QCD radiative corrections through virtual one loop gluon and real emission of gluons to the $q \bar{q} \rightarrow \gamma \gamma$ subprocess, would contribute to both SM and extra dimension models. The $q(\bar{q}) g \rightarrow q(\bar{q}) \gamma \gamma$ begins to contribute for both SM and extra dimension models at NLO. The LO $g g \rightarrow \gamma \gamma$ extra dimension process will also get one loop virtual gluon and real gluon emission radiative corrections. There will also be interference between the SM and extra dimension model to give contributions up to $\mathcal{O}(\alpha_s)$. In this analysis we have not included the $\mathcal{O}(\alpha_s)$ corrections as a result of the interference between the SM box diagram contribution and LO extra dimension contribution to the $g g \rightarrow \gamma \gamma$ subprocess, as it is quite suppressed in the region of interest to extra dimension models.

The $q(\bar{q}) g \rightarrow q(\bar{q}) \gamma \gamma$ NLO contribution has an additional QED collinear singularity when the photon gets collinear to the emitting quark and can be absorbed into the fragmentation function which gives the probability of a parton fragmenting into a photon. Parton fragmentation functions are additional non perturbative inputs which are not very well known. At the LHC, secondary photons as a result of hadron decaying into collinear photons and jets faking as photon are taken care of by photon isolation criteria [3, 4] which also substantially reduces the fragmentation contribution. Since the fragmentation is essentially a collinear effect, the fragmentation function can be avoided by the smooth cone isolation proposed by Frixione [16], which ensures that in no region of the phase space the soft radiation is eliminated. The smooth cone isolation is able to eliminate the not so well known fragmentation contribution and at the same time, ensures infrared safe (IR) observable. Centered in the direction of the photon in the pseudo rapidity (η) and azimuthal angle (ϕ) plane, a cone of radius $r = \sqrt{(\eta - \eta_\gamma)^2 + (\phi - \phi_\gamma)^2}$ is defined. The hadronic activity $H(r)$ is defined as the sum of hadronic transverse energy in a circle of radius $r < r_0$ and E_T^γ is the transverse energy of the photon. For all cones with $r \leq r_0$ the isolation criterion $H(r) < H(r)_{\max}$ has to be satisfied, where $H(r)_{\max}$ is defined as

$$H(r)_{\max} = \epsilon_\gamma E_T^\gamma \left(\frac{1 - \cos r}{1 - \cos r_0} \right)^n . \quad (3)$$

Efforts for the experimental implementation of the smooth cone isolation is on going.

Automation is an essential ingredient of this work. We have chosen to work in the aMC@NLO framework [17], which automatizes the MC@NLO formalism [13] to match NLO computations with parton showers. In this paper we present results matched to HERWIG [18]. For the NLO computation, isolation of IR poles and phase space integration are carried out by MadFKS [19], which automatizes the FKS subtraction method [20] using the MadGraph [21] matrix-element generator, whereas for one-loop amplitudes the results of Ref. [8] are used. The automation

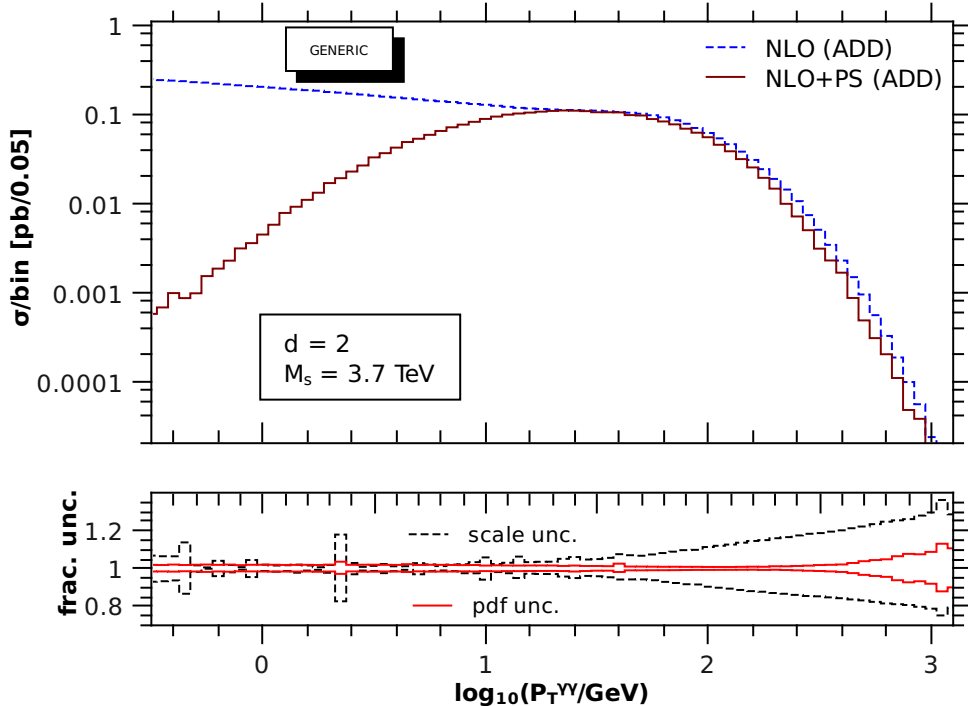


Figure 1: Transverse momentum distribution $p_T^{\gamma\gamma}$ of the diphoton for the fixed order NLO and NLO+PS. The ADD model parameters used are $d = 2$ and $M_S = 3.7$ TeV. The lower inset displays the scale and PDF, fractional uncertainties for the NLO+PS results.

within the MadGraph framework requires a new HELAS [22] subroutine to calculate helicity amplitudes with massive spin-2 particles [23, 24]. In addition, for our present analysis we have implemented the sum over the KK modes to take care of the virtual KK mode sum (Eq. 2) that contributes to process in the ADD model [24]. We use this framework to generate the events for 8 TeV run at the LHC. For the invariant mass distributions we have reproduced the results of [8] using the fixed order results from MadFKS. Also numerical cancellation of the singularities from the real and virtual terms have been explicitly checked.

3 Numerical results

In this section, we present the results for various kinematic distributions of photon pair in SM and ADD model. We have included all the subprocess contributions to NLO. The following input parameters are used: $\alpha_{em}^{-1} = 132.507$, $G_F = 1.16639 \times 10^{-5}$ GeV⁻², $m_Z = 91.188$ GeV and MSTW2008(n)lo68cl for (N)LO parton distribution functions (PDF) [25]. The MSTW PDF also sets the value of the strong coupling $\alpha_s(m_Z)$ at LO and NLO in QCD. The renormalisation and factorisation scales are

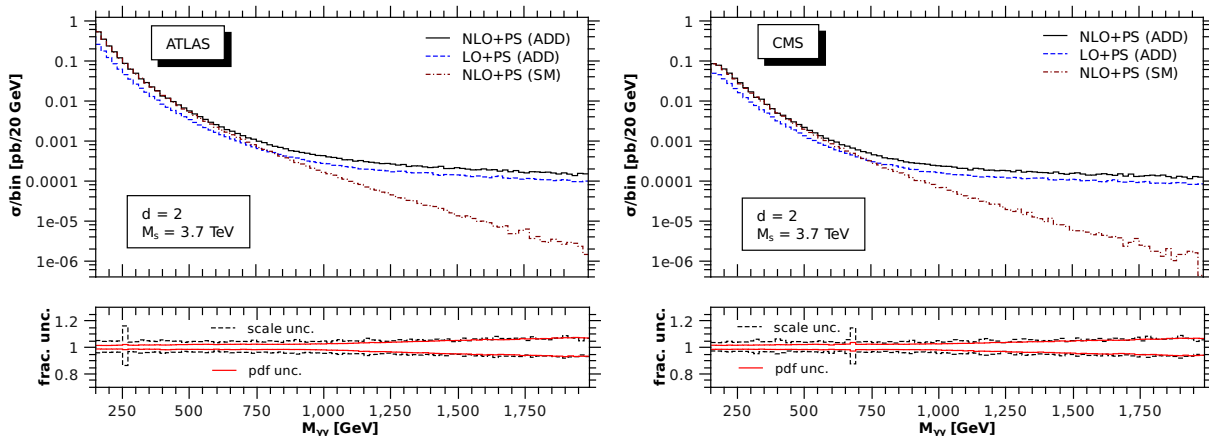


Figure 2: Invariant mass distribution $M_{\gamma\gamma}$ for ATLAS (left panel) and CMS (right panel) for $d = 2$ extra dimensions and $M_S = 3.7$ TeV. The SM contribution to NLO+PS and ADD to LO+PS and NLO+PS have been plotted. For the NLO+PS (ADD) results, the lower inset displays the scale and PDF fractional uncertainties.

chosen as $\mu_F = \mu_R = M_{\gamma\gamma}$, the invariant mass of the photon pair. The events that have to be showered are generated using the following generation cuts: $|\eta_{\gamma_{1,2}}| < 2.6$, $p_T^{\gamma_{1,2}} > 20$ GeV, diphoton invariant mass $100 \text{ GeV} < M_{\gamma\gamma} < M_S$ and the photon isolation is done using the Frixione isolation with $r_0 = 0.38$, $\epsilon_\gamma = 1$ and $n = 2$ (see Eq. (3)). More specific analysis cuts can be applied subsequently to generate the events.

The dependence of the prediction of an observable on the factorisation and renormalisation scales, is a result of the uncalculated higher order contributions, which can be estimated by varying μ_F and μ_R independently around the central value $\mu_F = \mu_R = M_{\gamma\gamma}$. The variation is done by the following assignment $\mu_F = \xi_F M_{\gamma\gamma}$ and $\mu_R = \xi_R M_{\gamma\gamma}$, where the values for (ξ_F, ξ_R) used are (1,1), (1/2,1/2), (1/2,1), (1,1/2), (1,2), (2,1), (2,2). The various ratios of μ_F , μ_R and $M_{\gamma\gamma}$ that appear as arguments of logarithms in the perturbative expansion to NLO are within the range $[1/2, 2]$. The variation of both μ_F and μ_R are taken as the envelope of the above individual variations. Variation of only μ_F would involve the choice $\xi_R = 1$ and varying ξ_F and vice-versa for variation of only μ_R . The PDF uncertainties are estimated using the prescription given by MSTW [25]. Fractional uncertainty defined as the ratio of the variation about the central value divided by the central value, is a good indicator of the scale and PDF uncertainties and is plotted in the lower insets to the various figures. As described in Ref. [15], the generation of these uncertainty bands can be done at virtually no extra CPU cost within the aMC@NLO framework.

To begin with, we compare the fixed order NLO result with NLO+PS for the transverse momentum of the diphoton $\log_{10} p_T^{\gamma\gamma}$ using generic cuts: $M_{\gamma\gamma} > 140$ GeV, $|\eta_\gamma| < 2.5$, $p_T^{\gamma_1} > 40$ GeV, $p_T^{\gamma_2} > 25$ GeV and $r_0 = 0.4$. In Fig. 1, $\log_{10} p_T^{\gamma\gamma}$ distribution is plotted for $d = 2$ with appropriate M_S value. It is clear that at low $p_T^{\gamma\gamma}$ values,

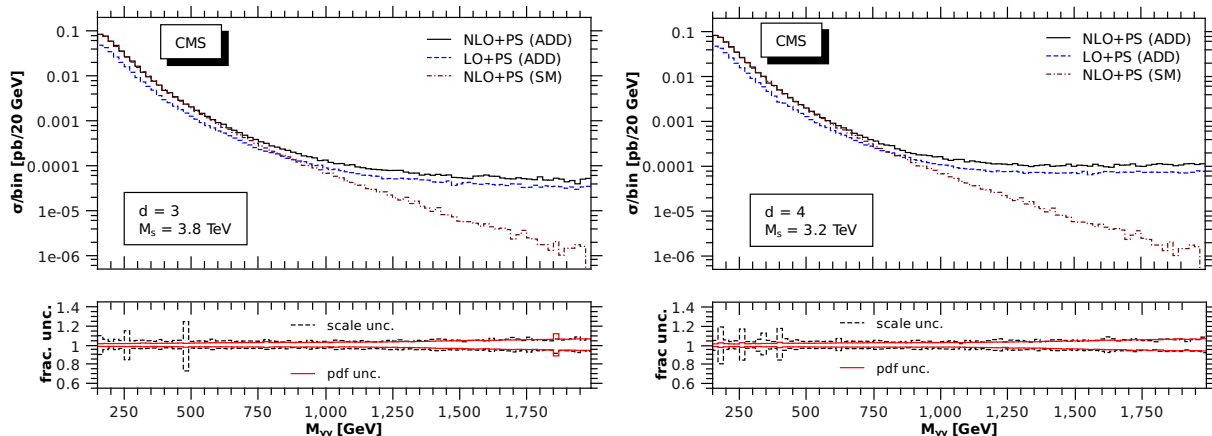


Figure 3: Invariant mass distribution for $d = 3$ (left panel) and $d = 4$ (right panel) is plotted for ADD and SM contributions to NLO+PS accuracy. The lower insets give the corresponding scale and PDF, fractional uncertainties for NLO+PS (ADD).

NLO+PS correctly resums the Sudakov logarithms, leading to a suppression of the cross section, while the fixed order NLO results diverges for $p_T^{\gamma\gamma} \rightarrow 0$. At high $p_T^{\gamma\gamma}$, the NLO fixed order and NLO+PS results are in agreement. In the lower inset of the Fig. 1, we have the scale and PDF variation of the NLO+PS, which increase with $p_T^{\gamma\gamma}$ as observed in [26].

We now present the results for the various kinematical distributions to NLO accuracy with PS (labelled as NLO+PS), for analysis specific cuts. Both the experiments ATLAS and CMS have looked for diphoton invariant mass in the region $140 \text{ GeV} < M_{\gamma\gamma} < M_S$. ATLAS cuts [3]: the rapidity of the individual photons are in the region $|\eta_\gamma| < 2.37$, with an exclusion region $1.37 < |\eta_\gamma| < 1.52$, the transverse momentum of the individual photons $p_T^\gamma > 25 \text{ GeV}$ and for photon isolation: sum of transverse energy of hadrons $\sum E_T(H) < 5 \text{ GeV}$ with $\Delta r < 0.4$. $\Delta r = \sqrt{\Delta\phi^2 + \Delta\eta^2}$ is a cone in the azimuthal angle, rapidity plane. For CMS the corresponding cuts are [4]: $|\eta_\gamma| < 1.44$, $p_T^\gamma > 70 \text{ GeV}$, photon isolation: (i) sum of the energy of hadrons $\sum E(H) < 0.05 E^\gamma$ with $\Delta r < 0.15$, (ii) sum of transverse energy of hadrons $\sum E_T(H) < 2.2 \text{ GeV} + 0.0025 E_T^\gamma$ with $0.15 < \Delta r < 0.4$. In addition to the ATLAS and CMS photon isolation, if we also include the Frixione isolation criteria, there is no appreciable change in the results.

In Fig. 2, we have plotted invariant mass distributions $d\sigma/dM_{\gamma\gamma}$ of photon pair in the SM as well as in the ADD model for ATLAS (left panel) and CMS (right panel). For ADD model we have obtained the distributions for $M_S = 3.7 \text{ TeV}$ and $d = 2$. The central value curves correspond to the choice $\mu_F = \mu_R = M_{\gamma\gamma}$, have been plotted for the ADD (NLO+PS) and purely SM (NLO+PS) contribution. The label ADD refers to the total contribution coming from SM, ADD and the interference between them. The corresponding ADD (LO+PS) contribution gives an indication of the quantitative impact of the NLO QCD correction. At larger invariant mass of

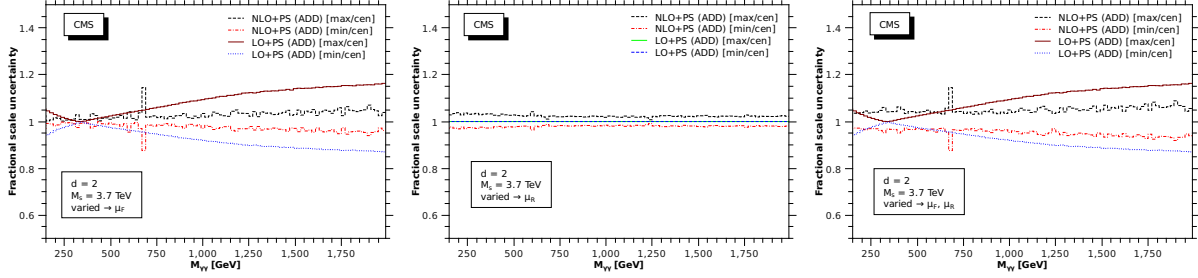


Figure 4: For the invariant mass distribution, with $d = 2$ and $M_S = 3.7$ TeV, the fractional uncertainties as a result of μ_F variation (left panel), μ_R variation (central panel) and μ_F , μ_R variation (right panel).

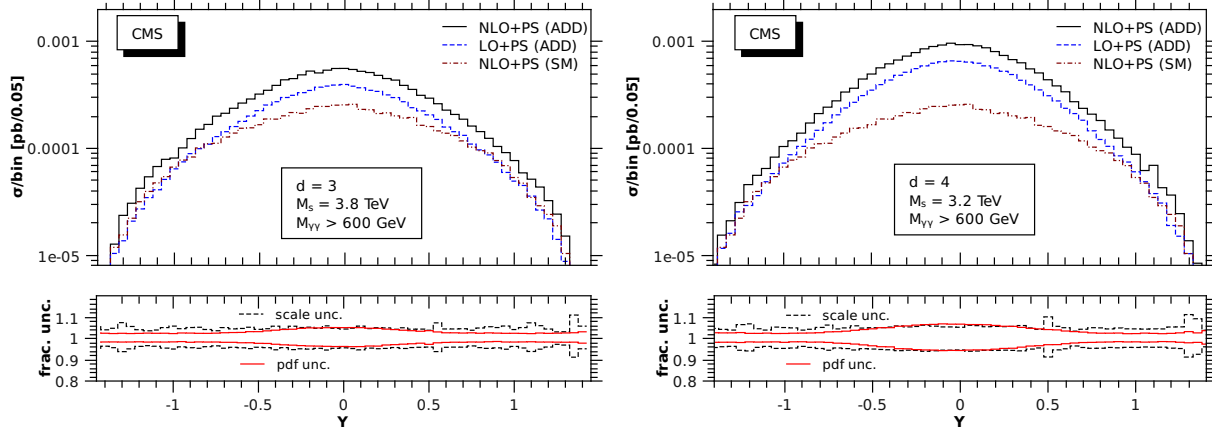


Figure 5: The rapidity (Y) distribution of the diphoton pair for $d = 3$ (left panel) and $d = 4$ (right panel) for SM (NLO+PS) and ADD (LO+PS and NLO+PS). The lower inset displays the corresponding fractional scale and PDF uncertainties of the NLO+PS (ADD) results.

the photon pair the ADD effect is dominant. To demonstrate the sensitivity of our predictions to the choice of scale and PDF uncertainties, in the lower inset fractional uncertainty by varying (a) both μ_F and μ_R and (b) PDF error sets, are plotted. The difference in the distribution in Fig. 2 for ATLAS and CMS can be attributed to the very different cuts used for their analysis. In Fig. 3, the corresponding plots for $d = 3, 4$ are plotted for the CMS cuts. The choice of M_S used for the plots corresponds to the lower bounds obtained by [3, 4] using the diphoton process. By including higher order corrections, the scale dependence goes down from about 25% at LO, to about 10% at NLO, as can be seen from the ratio plots. The PDF uncertainty does not change significantly and remains about 8%.

We now consider the fractional scale uncertainties on the invariant mass distribution as a result of the variation of the scales μ_F and μ_R (both independently

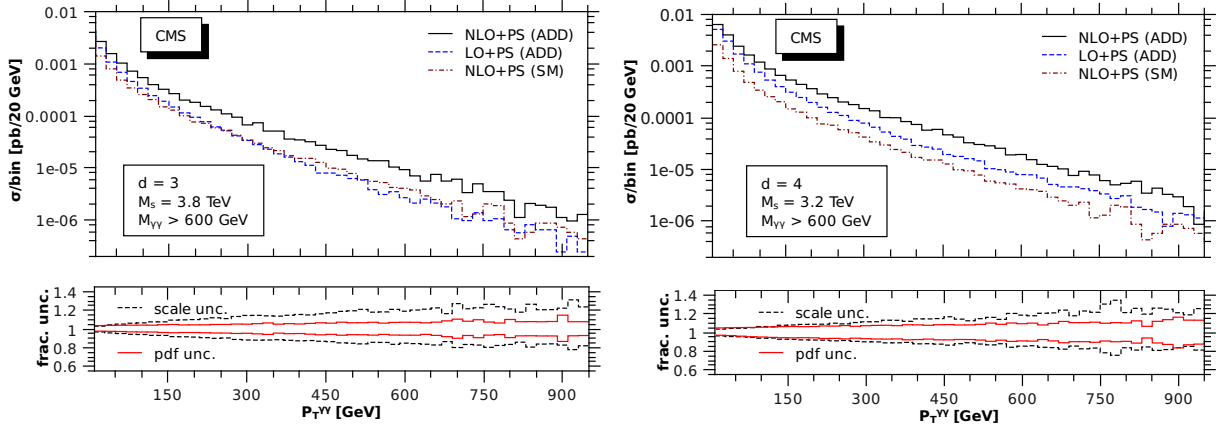


Figure 6: The transverse momentum distribution $p_T^{\gamma\gamma}$ of the diphoton for $d = 3$ (left panel) and $d = 4$ (right panel).

and simultaneously) in going from LO+PS to NLO+PS. Note that the LO cross sections depend only on μ_F through the PDF sets, but at NLO level the scale μ_R enters through $\alpha_s(\mu_R)$ and $\log(\mu_F/\mu_R)$ coming from the partonic cross sections after mass factorisation. As expected the inclusion of NLO QCD correction reduces the factorisation scale dependence resulting from the LO observable which is clear from Fig. 4 (left panel). In the high $M_{\gamma\gamma}$ region, the uncertainty of about 25% at LO+PS gets reduced to 5% when NLO+PS corrections are included. On the other hand, the μ_R dependence enters only at NLO level (see middle panel of Fig. 4) which will get reduced only if NNLO corrections are included. Hence, we see our NLO corrections are sensitive to the choice of μ_R but the variation is only 5% and is fairly constant for the range of invariant mass considered. If we vary both μ_F and μ_R simultaneously as shown in Fig. 4 (right panel), we find that the reduction in the μ_F scale dependence at NLO level is mildly affected by the μ_R variation in the large invariant mass region. In the small invariant mass region, the LO and NLO results exhibit smaller μ_F dependence compared to the large invariant mass region. But μ_R dependence coming from the NLO results does not change much with the invariant mass $M_{\gamma\gamma}$. Hence variation due to μ_R at small $M_{\gamma\gamma}$ is larger compared to that resulting from μ_F . This explains the behavior at small invariant mass regions where the NLO+PS variation is in excess of the LO+PS (see right panel of Fig. 4).

The rapidity distribution of the diphoton pair is plotted in Fig. 5 for $d = 3$ (left panel) and $d = 4$ (right panel). For this analysis we have chosen $M_{\gamma\gamma} > 600$ GeV, the region where the effects of ADD model begins to dominate over the SM diphoton signal at NLO (see Fig. 3). The scale and PDF uncertainties to NLO are displayed as insets at the bottom of each figure. The scale uncertainties are usually larger than the PDF uncertainties in the rapidity distribution except for the central rapidity region where they are comparable. For $d = 3$ the scale uncertainties are about 20% around the central rapidity region, which come down to about 10%

when NLO+PS corrections are included. The PDF uncertainties for LO+PS and NLO+PS are comparable.

Finally, we plot the transverse momentum distribution in Fig. 6 for $d = 3$ (left panel) and $d = 4$ (right panel), for the SM and ADD model to NLO+PS accuracy, with $M_{\gamma\gamma} > 600$ GeV. The ADD results are also plotted for LO+PS. The scale and PDF uncertainties are displayed as insets at the bottom of the plots for NLO+PS (ADD).

4 Conclusion

In this analysis, we have presented the diphoton final state in the large extra dimension model to NLO in QCD and matching to parton shower is implemented using the aMC@NLO framework. All the subprocesses that contribute to the diphoton final state from both the SM and ADD model are considered to NLO in QCD. This is the first time MC@NLO formalism has been used for a processes in the ADD model and we hope it would significantly help extra dimension searches at the LHC to constrain the ADD model parameters. Using a set of generic cuts we first demonstrated the importance of NLO+PS over the fixed order NLO computations, by considering the $p_T^{\gamma\gamma}$ distribution. We have presented our results for various observables *viz.*, invariant mass, rapidity and transverse momentum of the diphoton, both for the ATLAS and CMS detector specific cuts to NLO+PS accuracy. It is important to note that there is substantial enhancement of the various distributions due to the inclusion of NLO corrections and both the theoretical and PDF uncertainties have been estimated. There is a significant decrease in theoretical uncertainties from over 20% at LO to about 10% when NLO corrections are included. The results are presented for different number of extra spatial dimensions $d = 2 - 6$ and the respective values of fundamental scale M_S that have been experimentally bounded. The event files for $d = 2 - 6$ are available on the website <http://amcatnlo.cern.ch> and we are working on making the code that was used to generate these events publicly available.

Acknowledgements

PM and VR would like to acknowledge M. C. Kumar and Anurag Tripathi for previous collaboration on diphoton parton level results. SS would like to acknowledge useful communication with Priscila de Aquino and Fabio Maltoni. SS would like to thank UGC, New Delhi, for financial support. MZ would like to thank Fabio Maltoni for reading the manuscript and for many inspiring discussions. The work of MZ is supported by the 4.4517.08 IISN-FNRS convention.

References

- [1] N. Arkani-Hamed, S. Dimopoulos and G. Dvali, Phys. Lett. B 429 (1998) 263; I. Antoniadis, N. Arkani-Hamed, S. Dimopoulos and G. Dvali, Phys. Lett. B 436 (1998) 257; N. Arkani-Hamed, S. Dimopoulos and G. Dvali, Phys. Rev. D59 (1999) 086004.
- [2] L. Randall and R. Sundrum, Phys. Rev. Lett. 83 (1999) 3370.
- [3] ATLAS Collaboration, Phys. Lett. B710 (2012) 538.
- [4] CMS Collaboration, arXiv: 1112.0688 [hep-ex]
- [5] T. Han, J. D. Lykken and R. J. Zhang, Phys. Rev. D59 (1999) 105006
- [6] G. F. Giudice, R. Rattazzi, and J. D. Wells, Nucl. Phys. B544 (1999) 3.
- [7] P. Mathews, V. Ravindran, K. Sridhar and W. L. van Neerven, Nucl. Phys. B713 (2005) 333; P. Mathews, V. Ravindran, Nucl. Phys. B753 (2006) 1; M.C. Kumar, P. Mathews, V. Ravindran, Eur. Phys. J. C49 (2007) 599.
- [8] M.C. Kumar, P. Mathews, V. Ravindran, A. Tripathi, Phys. Lett. B672 (2009) 45; Nucl. Phys. B818 (2009) 28.
- [9] N. Agarwal, V. Ravindran, V. K. Tiwari, and A. Tripathi, Nucl. Phys. B 830, 248 (2010); Phys. Rev. D 82, 036001 (2010).
- [10] S. Karg, M. Karamer, Q. Li, and D. Zeppenfeld, Phys. Rev. D 81, 094036 (2010).
- [11] X. Gao, C. S. Li, J. Gao, and J. Wang, Phys. Rev. D 81, 036008 (2010).
- [12] M. C. Kumar, P. Mathews, V. Ravindran, and S. Seth, Nucl. Phys. B847, 54 (2011); J. Phys. G 38, 055001 (2011).
- [13] S. Frixione, B. R. Webber, JHEP 06 (2002) 029.
- [14] P. Nason, JHEP 11 (2004) 040.
- [15] R. Frederix, S. Frixione, V. Hirschi, F. Maltoni, R. Pittau and P. Torrielli, JHEP 02 (2012) 099.
- [16] S. Frixione, Phys. Lett. B 429, 369 (1998).
- [17] R. Frederix, S. Frixione, V. Hirschi, F. Maltoni, R. Pittau, P. Torrielli, Phys. Lett. B701 (2011) 427.
- [18] G. Corcella, I. G. Knowles, G. Marchesini, S. Moretti, K. Odagiri, P. Richardson, M. H. Seymour and B. R. Webber, JHEP 01 (2001) 010.

- [19] R. Frederix, S. Frixione, F. Maltoni, T. Stelzer JHEP 0910 (2009) 003.
- [20] S. Frixione, Z. Kunszt, and A. Signer, Nucl. Phys. B467 (1996) 399.
- [21] J. Alwall, M. Herquet, F. Maltoni, O. Mattelaer, T. Stelzer, JHEP 1106 (2011) 128.
- [22] H. Murayama, I. Watanabe, K. Hagiwara, KEK-91-11.
- [23] K. Hagiwara, J. Kanzaki, Q. Li, K. Mawatari, Eur. Phys. J. C56 (2008) 435.
- [24] P. de Aquino, K. Hagiwara, Q. Li, F. Maltoni, JHEP 06 (2011) 132.
- [25] A. D. Martin, W. J. Stirling, R. S. Thorne, and G. Watt, Eur. Phys. J. C63 (2009) 189285.
- [26] P. Torrielli and S. Frixione, JHEP 04 (2010) 110.